

Electron-Ion Temperature Relaxation Models for Inertial Confinement Fusion

Barry Xu

Brighton High School
Rochester, NY

Advisor: S.X. Hu

Laboratory for Laser Energetics
University of Rochester
Rochester, NY
November 2010

1 Introduction

At the Laboratory for Laser Energetics (LLE) at the University of Rochester and the National Ignition Facility (NIF) in Livermore, California, research is being focused on the process and application of laser fusion. While there are two main methods of laser fusion, direct and indirect drive, the Laboratory for Laser Energetics mainly deals with direct drive fusion, a process that directly irradiates a target, using the 60-beam OMEGA laser system.

During direct drive, inertial confinement fusion (ICF) is a process in which a cryogenic target is irradiated by high intensity pulses from a laser. The target is a spherical plastic (CH) capsule, approximately 10 μm thick with a diameter of $\sim 860 \mu\text{m}$, coated with approximately 65 μm of deuterium-tritium (DT) ice, and filled with three atmospheres of DT. During ICF, the laser pulses partially ablate the CH and deliver the energy necessary to implode the target shell, through the “rocket” effect. This effect compresses the target through laser-driven shocks and spherical convergence [1, 2].

The result is the creation of three distinct regions of particles. Plasma is formed and ejected by the target, creating a high temperature, low density corona around the target. The next region is the (relatively) low temperature and high density shell, which is followed by the hotspot center, which is high temperature and medium density. All three parts are created in about four nanoseconds on the OMEGA laser system and about twelve nanoseconds for the NIF designs.

When the laser irradiates the target, most of the energy is absorbed by the inverse bremsstrahlung process, in which electrons oscillating in the laser electric field undergo momentum transfer collisions with the ions that convert their oscillating energy to

thermal energy. The inverse bremsstrahlung absorption rate is proportional to this collision rate, which is directly proportional to the Coulomb logarithm.

The Coulomb logarithm is a coefficient that helps to model the electron-ion relaxation rate. However, four different models have been proposed for calculating the Coulomb logarithm, the Spitzer model, the Lee-More Model, the Molecular Dynamic (MD) model, and the Brown-Preston-Singleton (BPS) model. Each model calculates the Coulomb logarithm using a different method, such as considering quantum degeneracy effects and using classical molecular dynamics.

These simulations were focused mainly on determining which model most accurately predicted fusion results and the best gain. A program was written to be used with hydrodynamic simulations using triple-picket pulse designs for both the LLE and NIF designs. Also, each model was used to calculate the neutron yield, the laser absorption, the compression areal density ρR , and the neutron production rate.

2 Simulation Models

2.1 *Electron-Ion Relaxation Rate*

When the electrons first absorb the laser energy, they must then transfer that energy to the ions in order for fusion to occur. This electron-ion temperature relaxation rate is defined as:

$$\frac{dT_{e/i}}{dt} = \nu \cdot (T_i - T_e) \Rightarrow \nu = \nu_o \cdot \ln \Lambda \quad (1)$$

where $\ln \Lambda$ is the Coulomb logarithm and the prefactor, ν_o , is a function of density, charge and mass given by

$$v_o = \frac{8}{3} \cdot n_i e^4 Z^2 \frac{\sqrt{2\pi m M}}{(m k_B T_i + M k_B T_e)^{3/2}} \quad (2)$$

where M and m are the ion and electron masses, respectively, T_i and T_e are the ion and electron temperatures, Z and e are the ion and electron charges, n_i is the ion density, and k_B is the Boltzman Constant [2, 4].

The Coulomb logarithm in the above equation is a unit-less coefficient. This helps to characterize the long range and short range electron-ion collisions in plasmas. The main issue is that the Coulomb logarithm has been approximated in four distinct ways, using various expressions. This leads to debate over which model is most accurate. In the next section, each model is given and analyzed.

2.2 Coulomb Logarithm expressions

Four different equations for the Coulomb logarithm have been examined in these calculations. The first one is the Spitzer equation, proposed in 1953, given by:

$$\ln \Lambda = \ln \left(\frac{3}{2 Z_e Z_i e^3} \sqrt{\frac{k_B^3 T_e^3}{\pi m_e}} \right) \quad (3)$$

where Z_e and Z_i are the electron and ion charge, with Z_e equal to one [3]. This equation was created to mitigate the problem of integral divergence in binary collisions. Also, a cut-off was introduced to some of the impact parameters.

The second model that was analyzed is the Lee-More model, proposed in 1984 [5]. Their model includes electron degeneracy effects for low temperature plasmas and is given by:

$$\ln \Lambda = \frac{1}{2} \ln \left[1 + (b_{\max}^2 / b_{\min}^2) \right] \quad (4)$$

The distance b_{\max} is defined as the Debye-Hückel screening length, λ_{DH} , with degeneracy modification, defined as:

$$\frac{1}{\lambda_{DH}} = \sqrt{\frac{4\pi n_e e^2}{k_B \sqrt{T_e^2 + T_F^2}} + \frac{4\pi n_i Z^2 e^2}{k_B T_i}} \quad (5)$$

where T_F is the Fermi degeneracy temperature. This gives the largest impact parameter for classical collisions. The smallest impact parameter, b_{\min} , on the other hand, is the larger of the classical collision distance and the de-Broglie wavelength of thermal electrons:

$$b_{\min} = \max\left(\frac{Ze^2}{3k_B T_e}, \frac{\hbar}{2\sqrt{3mk_B T_e}}\right) \quad (6)$$

The Lee-More model for the Coulomb logarithm is implemented into the hydrocodes LILAC [7] and DRACO [8] that are being used at LLE for implosion simulations.

In 2008, the relaxation rate problem was revisited for ICF plasma conditions by Dimonte and Daligault [4]. Their calculations incorporated classical¹ molecular dynamic simulations for electron-ion plasmas with like charges. They came up with a coupling parameter, g , for their expression of the Coulomb Logarithm:

$$\ln \Lambda = \ln\left(1 + \frac{0.7}{g}\right) \quad (7)$$

The parameter “ g ” is the ratio between the smallest and the largest impact parameter, defined as:

$$g = \frac{R_c}{\lambda_D} = \frac{Ze^2}{\lambda_D k_B T_e} \quad (8)$$

¹ The classical model is derived from Newton’s laws and equations.

where R_c , the Landau length, characterizes large angle scatterings, representing the smallest impact parameter. The electron Debye length, λ_D , is the largest impact parameter, with the fields at larger distances being screened out [4].

The fourth and final model examined was the model proposed by Brown, Preston, and Singleton (BPS) in 2009. In contrast to numerical simulations, analytical studies using dimensional continuation resulted in a BPS model for a wide range of plasma conditions, including quantum and coupling effects. The BPS formula is comprised of three terms [6], a main term and two correction factors, shown here:

$$\ln \Lambda_{BPS} = \ln \Lambda_{BPS}^{QM} + \ln \Lambda_{BPS}^{\Delta C} + \ln \Lambda_{BPS}^{FD} \quad (9)$$

The leading term is based on quantum mechanics and accounts for quantum effects. The second term is a correction for when the plasma parameters are not near the quantum limit; and the third term takes into account the many-body electron degeneracy effects when Fermi-Dirac statistics become important. Each term, ignoring small electron-ion mass ratio effects, can be given as:

$$\ln \Lambda_{BPS}^{QM} = \frac{1}{2} \left[\ln \left(\frac{8k_B^2 T_e^2}{\hbar^2 \omega_e^2} \right) - \gamma - 1 \right], \quad (10)$$

$$\ln \Lambda_{BPS}^{\Delta C} = -\frac{\varepsilon_H}{k_B T_e} \sum_i \frac{Z_i^2 \omega_i^2}{\omega_i^2} [1.20205 \times \left[\ln \left(\frac{k_B T_e}{Z_i^2 \varepsilon_H} \right) - \gamma \right] + 0.39624] \quad (11)$$

$$\ln \Lambda_{BPS}^{FD} = \frac{n_e \lambda_e^3}{2} \left[\frac{-1}{2} \left(1 - \frac{1}{2^{3/2}} \right) \times \left\{ \ln \left(\frac{8k_B^2 T_e^2}{\hbar^2 \omega_e^2} \right) - \gamma - 1 \right\} + \left(\frac{\ln 2}{2} + \frac{1}{2^{5/2}} \right) \right] \quad (12)$$

where ε_H is the binding energy of hydrogen, \hbar is the Planck constant, and γ is the Euler constant². The electron and ion plasma frequencies are given by ω_e and ω_i , respectively;

² The Euler constant ≈ 0.57721 .

and ω_i is the average ion frequency. BPS also included an electron thermal wavelength, λ_e , which is a derivative of the thermal de-Broglie wavelength [6].

Each model was then run through simulations using the hydro-code LILAC, as described in the next section. Then based on the results, a model was proposed to most accurately model the Coulomb logarithm.

2.3 *Implementation into the LILAC Code*

Each of the above mentioned models was implemented into the 1-D hydro-code, LILAC. A subroutine was written using the FORTRAN programming language. The program differentiated between the various regions of the reaction area, the hotspot, the shell, and the coronal plasma.

Each model was run through simulations with varying electron and ion temperatures, modeling the approximate temperatures for the three regions. After the Coulomb logarithm was calculated for each region, the program was run and calculated the various output data using the information from an OMEGA cryogenic shot and the NIF designs for the triple-picket pulse shape.

3 **Results and Analysis**

3.1 *Predicted Coulomb Logarithm*

The program was run for the following conditions: a) $T_e = 5$ keV and $T_i = 10$ keV, which models the “hotspot” center during shock convergence for the NIF designs; b) $T_e = 2.5$ keV and $T_i = 5$ keV, which models the “hotspot” center during the shock convergence for the OMEGA designs; c) $T_e = 2$ keV and $T_i = 1$ keV, which models the typical corona temperatures for an OMEGA shot; and d) $T_e = 50$ eV and $T_i = 100$ eV, which models the imploding shell conditions for an OMEGA target.

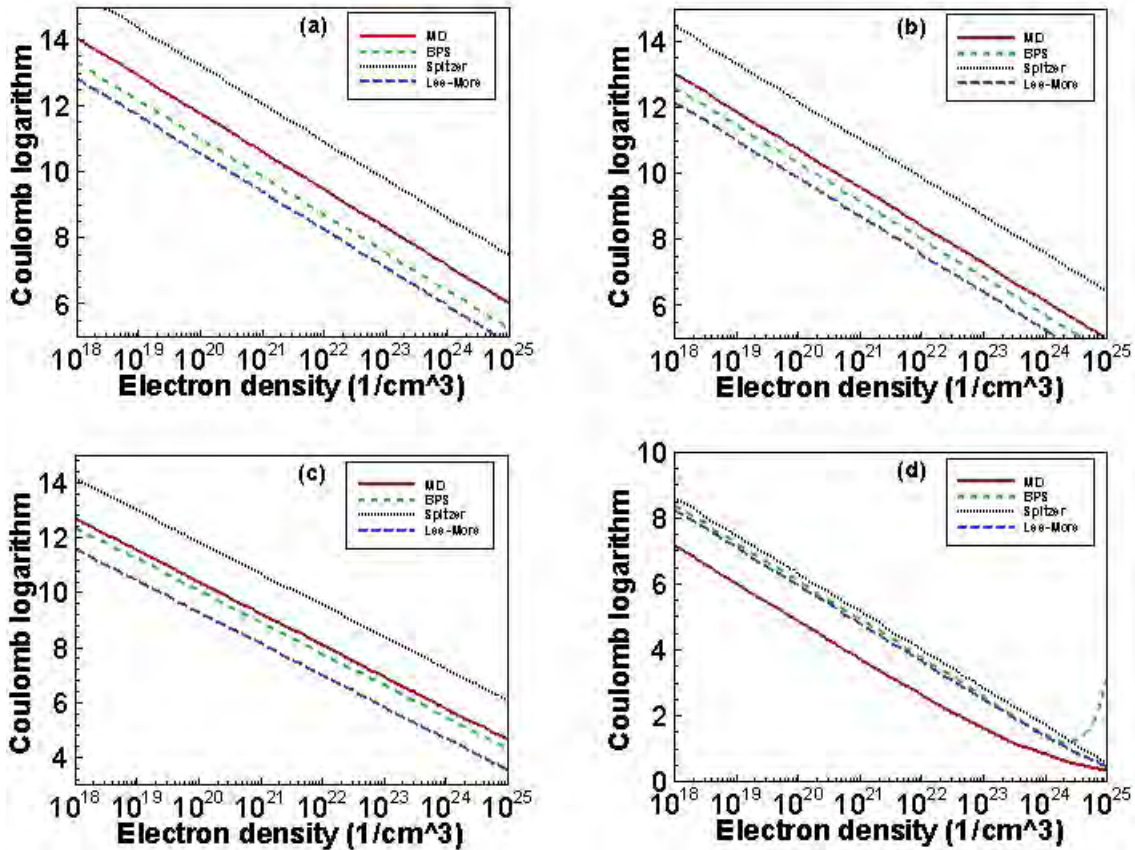


Figure 1: The Coulomb Logarithm calculated for various conditions

The Coulomb logarithm as a function of electron density for the four different electron-ion temperature relaxation rates at different plasma temperatures. a) $T_e=5$ keV and $T_i=10$ keV, b) $T_e=2.5$ keV and $T_i=5$ keV, c) $T_e=2.0$ keV and $T_i=1.0$ keV, and d) $T_e=50$ eV and $T_i=100$ eV

From this data, the Spitzer model predicted the highest Coulomb logarithm for almost all temperatures and densities. Also, in Fig 1(a) and 1(b), the difference between the two newer models and the Lee-More model was consistently $\sim 10\%$. For temperatures above 1 keV, the BPS and MD models were generally within 5-7% of each other. In Fig. 1(c), which shows the typical coronal temperatures, the MD and BPS models produced very similar results, which are $\sim 15\%$ higher than the standard Lee-More model prediction near the critical density regime ($n_e \sim 9.1 \times 10^{21}$ electrons/cm³) of OMEGA's UV laser ($\lambda = 0.351$ μm). This difference in $\ln\Lambda$ affects the amount of laser absorption in the corona, subsequently affecting target performance.

Inside the target shell, the temperature is ~ 100 eV during the implosion, where the DT plasma is moderately coupled and partially degenerate [9]. At this point, it is expected that quantum and many-body effects start becoming important; for such conditions, Fig. 1(d) shows that the BPS and the Lee-More models are very similar, but the classical MD model deviates from this, making it no longer valid. The BPS calculation, in Fig. 1(d), shows an increase for very high densities, which clearly shows the degeneracy effects because the plasma temperature is well below the Fermi temperature.

3.2 Hydro-Simulation Result: OMEGA

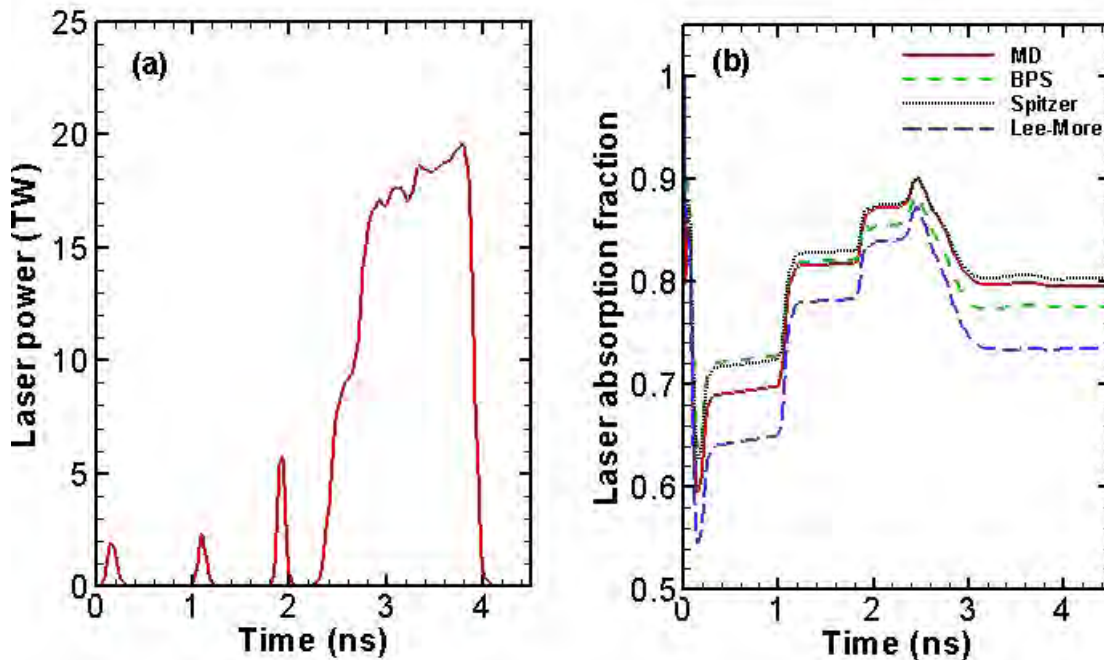


Figure 2: Pulse Shape and Laser Absorption for the OMEGA system

These graphs show a) the laser pulse shape for cryogenic DT implosions on OMEGA using three initial shocks to induce a compression shockwave and a fourth to implode the shell; b) the time-dependent laser absorption predicted by the four models.

These models were implemented and then simulated using a triple picket plus a main step pulse shape, for both the OMEGA facility and the direct drive NIF designs, to implode the cryogenic target [10]. Fig. 2(a) shows the exact pulse shape for the OMEGA shot. The first three pickets shot at the target start shock waves that propagate through the shell and coalesce causing it to compress inward. This places the target into the appropriate adiabat ($\alpha \sim 2$) and gives the target a high compression areal density $\rho R \sim 300$ mg/cm² [10]. The OMEGA simulation results are plotted in Figs. 2 and 3. Laser absorptions predicted by the different models are displayed in Fig. 2(b), with the Lee-More model predicting the least amount of absorption. This is expected because Fig. 1(c) predicts the Lee-More model calculating the smallest Coulomb logarithm for the coronal plasma.

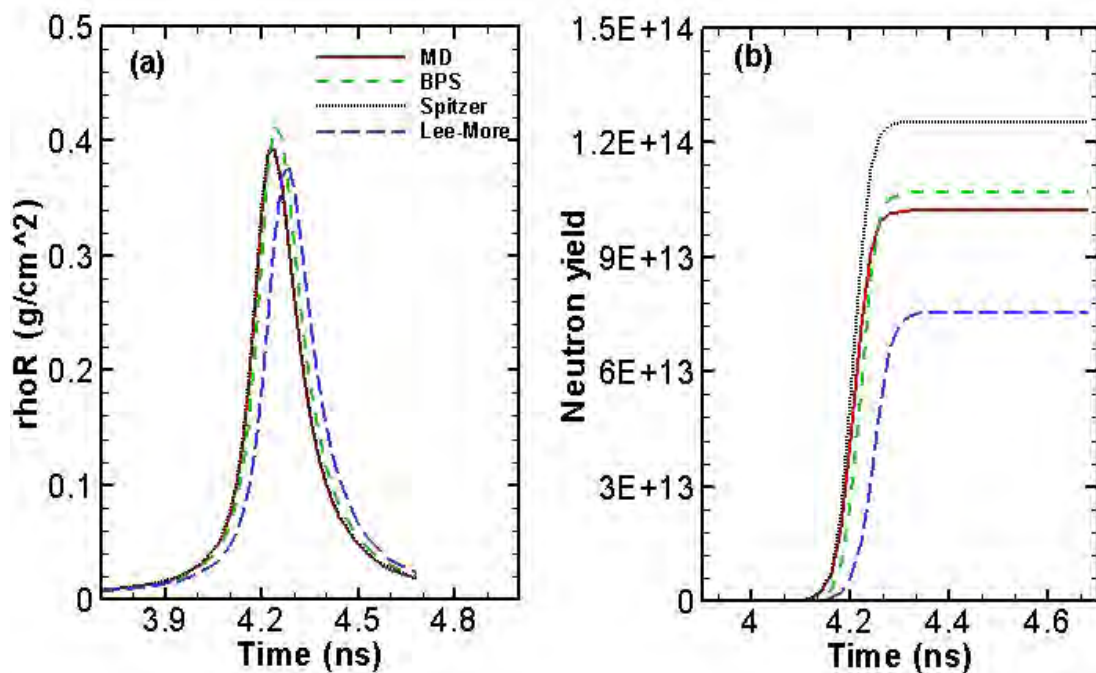


Figure 3: Graphs of ρR and neutron yield
 Each of these graphs show the predicted value for ρR and neutron yield as functions of time. a) ρR is the density times the radius and is a measure of the compression; b) this is the predicted neutron yield for each model, with the Spitzer model predicting the most.

A point of interest is that the inverse bremsstrahlung absorption is linearly proportional to the Coulomb logarithm. At the end of the main pulse, in Fig. 2(b), the classical MD result is the closest to the Spitzer result. This is expected since both the Spitzer and MD equations are based on the Newtonian model of particle interactions. The BPS model appears between the Lee-More and the MD models. The difference in absorption can be as high as 7%, which is a measurable difference in experiments.

The corresponding compression areal density ρR and the neutron yield are shown in Fig. 3(a) and Fig. 3(b), respectively. Compared to the Lee-More model, all of the models have a higher peak ρR , and the peak occurs earlier for all of them than the Lee-More model. This is consistent with the higher absorption, as seen in Fig. 2(b). For neutron yield, both the BPS and MD models predict similar outputs, but both differ from the Lee-More model by $\sim 30\%$. Again, this difference in neutron yield constitutes a measurable difference in experiments.

Based on the results from the OMEGA data, the Spitzer model appears to predict a value of the Coulomb logarithm that is too high. Also, the Lee-More model seems to predict too low a value. This can be attributed to the fact that these models do not take into account all of the same effects as the BPS and MD models, both of which predict moderate values for the Coulomb logarithm and, in turn, moderate values for the neutron yield.

3.3 *Hydro-Simulation Results: NIF*

The results from the LILAC simulations using the direct-drive NIF designs suggested a similar outcome. However, it is worth noting that the targets used by the NIF differ from the targets used by the OMEGA facility. Mainly, the target is bigger; the deuterated plastic shell is $\sim 37 \mu\text{m}$ with $\sim 150 \mu\text{m}$ DT ice. This is because the NIF can

deliver more energy to the target, as evidenced by the pulse shape shown in Fig. 4(a), which lasts 2.5 times longer than the OMEGA system and has a much higher peak power.

Fig. 4(b) shows that the total amount of laser absorption is $\sim 95\%$ for all four models. This can be attributed to the fact that, on the NIF, the plasma density scale length is longer than on OMEGA, resulting in more laser absorption. Fig 4(b) shows that the Lee-More model predicts a lower amount of absorption, especially during the first picket. This would affect the neutron production because the amount of compression the target undergoes is proportional to the amount of energy absorbed.

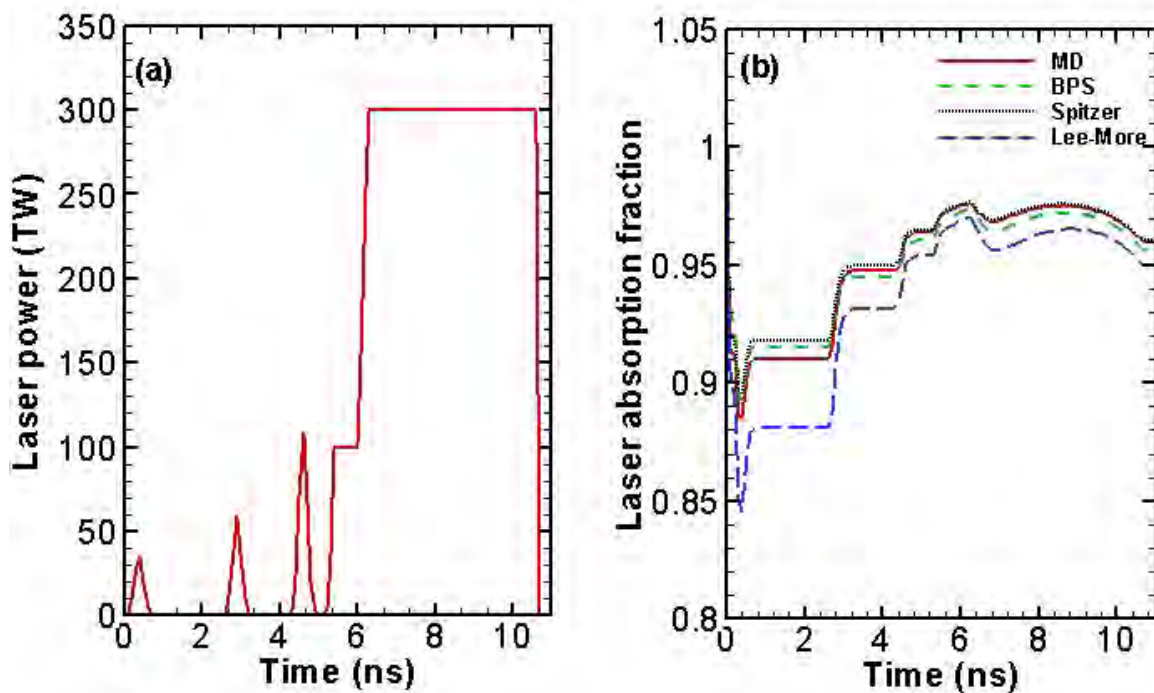


Figure 4 Pulse Shape and Laser Absorption on the NIF designs

These graphs show a) the laser pulse shape for the NIF designs is time dependent; b) the laser absorption predicted by each model for the NIF designs.

Compression ρR is shown in Fig. 5(a). The variations in peak ρR can be accounted for by the differences in shock dynamics. Fig 5(b) shows the neutron yield for the NIF simulations. Again, because all of the predicted laser absorption percentages are

so close together [see Fig. 4(b)], the variations between the predicted neutron yields are relatively small. Based on the neutron yield, the gain (the ratio between the total energy output and the total input energy) predicted by each of the models can be seen in Table 1. There is a variation of ~9% between all of the models.

Table 1 Calculated gains for each of the proposed models.

Model	Spitzer	Lee-More	MD	BPS
Gain	48.2	45.5	49.5	49.3

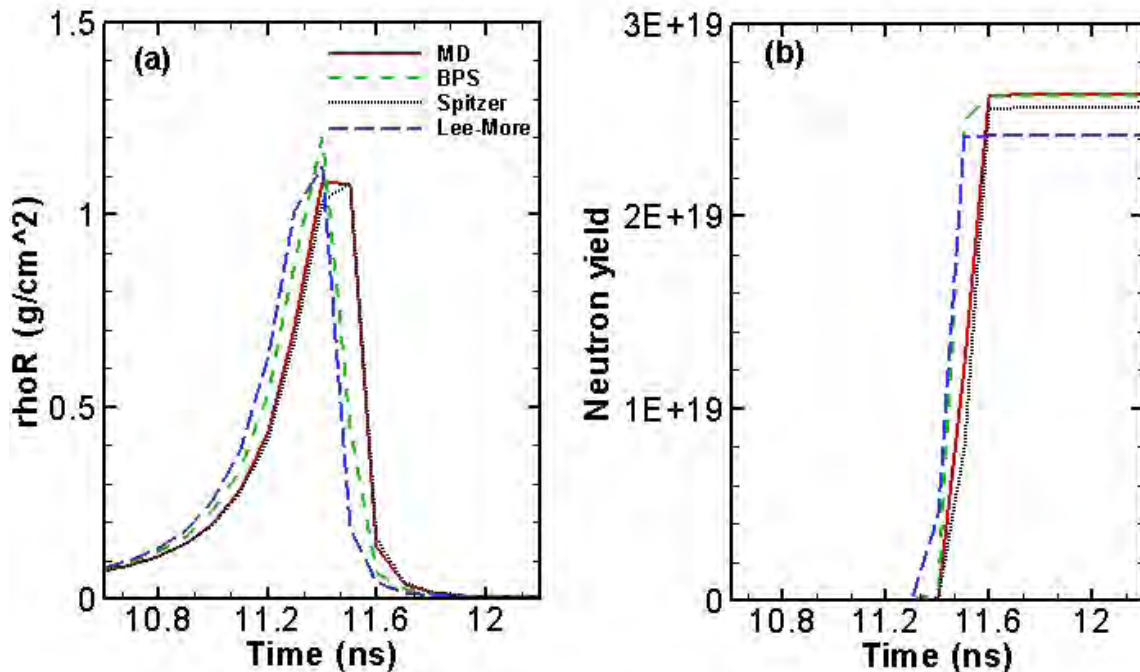


Figure 5 The areal density and the neutron yield for the NIF designs
 These graphs display a) the areal density, ρR in g/cm^2 and b) the neutron yield predicted.

3.4 Proposed Model

From the results obtained and the analysis of the models, a “best-fit” model was determined for calculating the Coulomb logarithm. As the coronal hotspot temperatures increase above 2 keV for ICF implosions, the MD simulations, which were performed in an ab initio fashion, should better characterize the processes at lower densities. This is due to the fact that these lower density regions behave more according to classical

thermal equilibrium processes, which the MD model accurately accounts for. On the other hand, the BPS formula accounts for the moderately coupled and partially degenerate plasmas in the low-adiabat shell, making it more applicable for those conditions.

Therefore, a combined model for the Coulomb logarithm would be the most accurate. The classical MD model would be used for plasma electron densities less than the critical density, n_c , the maximum density that can be achieved by a 351-nm laser, $\sim 1 \times 10^{22}$ e/cm³, and the BPS formula for the dense shell.

$$\ln \Lambda = \begin{cases} \ln \Lambda_{BPS} & (n_e > n_c) \\ \ln \Lambda_{MD} & (n_e < n_c) \end{cases} \quad (13)$$

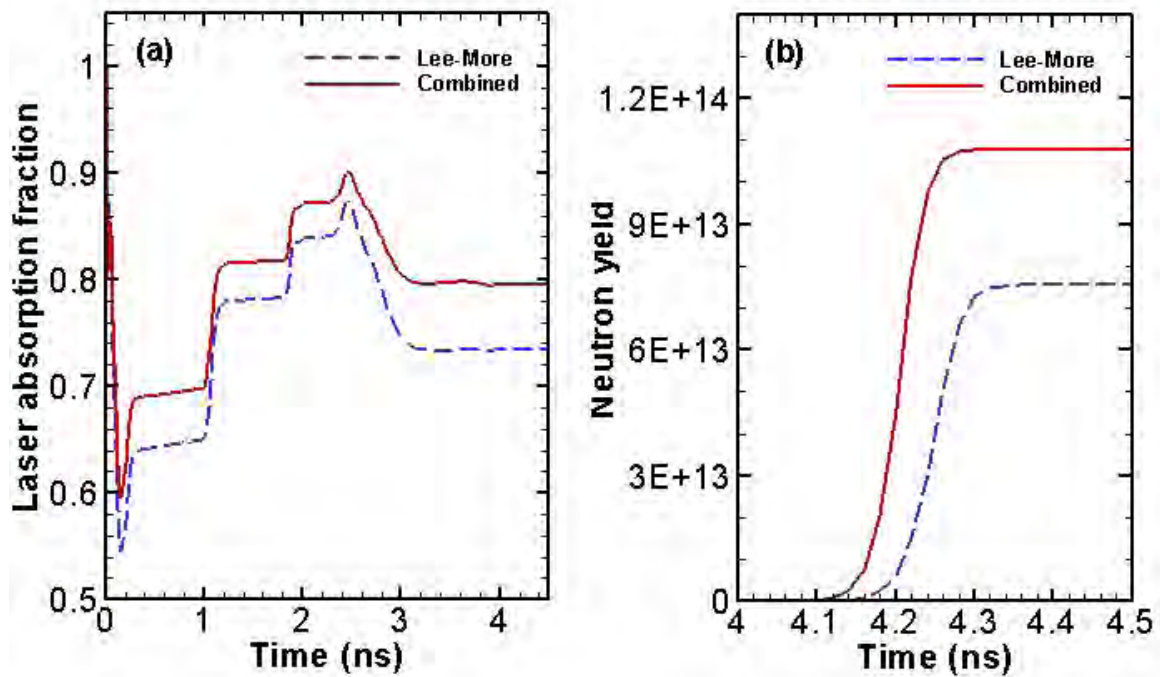


Figure 6 The proposed model compared with the Lee-More model for OMEGA
 These graphs show a) the laser absorption fraction and b) the predicted neutron yield, for both the proposed model and the Lee-More model.

Using this combined model, OMEGA implosions, discussed in Figs. 2 & 3, and NIF implosions, discussed in Figs. 4 & 5, have been simulated. The simulation results are shown in Figs. 6-9 and are shown with the Lee-More model for comparison. The laser absorption, which is plotted in Fig 6(a), shows that the combined model predicts ~6% higher absorption than the Lee-More model. Consequently, the Combined model predicts ~30% larger neutron yield than the Lee-More model, which is a significant increase.

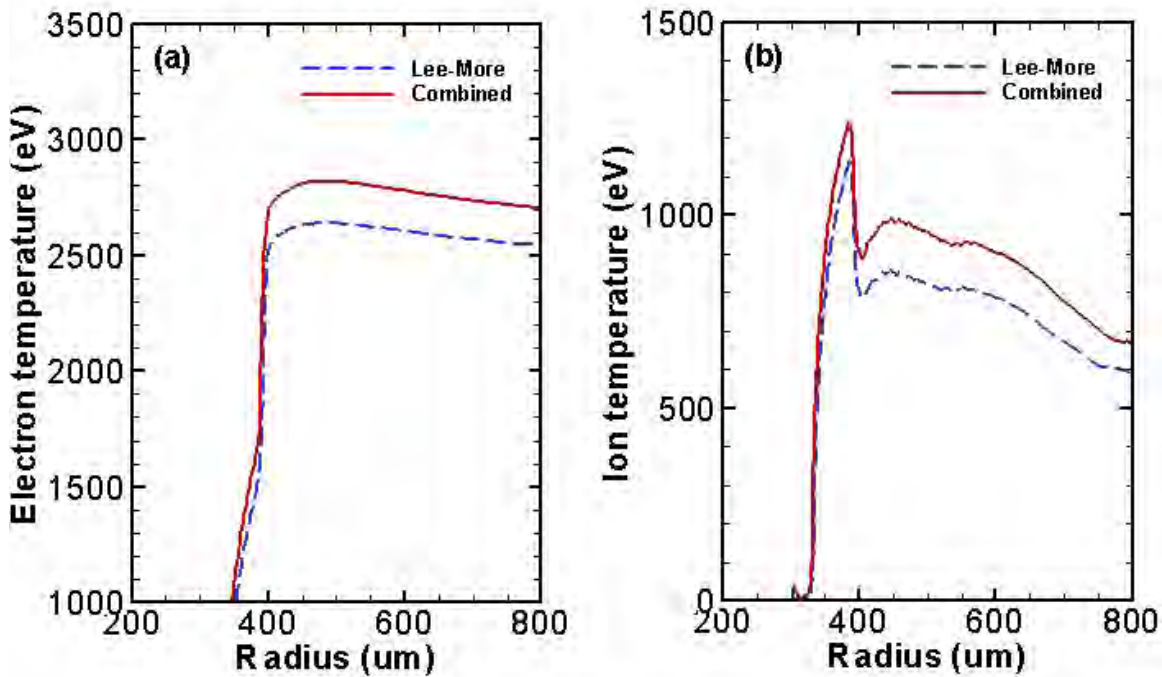


Figure 7 Predicted temperatures by the proposed model and the Lee-More model for OMEGA
 These two graphs show a) the electron temperature and b) the ion temperatures predicted by the models as a function of radius. This is important because it affects the overall performance of the shot.

Also, it is worth noting that the coronal electron and ion temperatures are quite different for the two models. Fig. 7 shows that at $t = 3.0$ ns, which is just after the main pulse has started to irradiate the target, there is a difference of ~10% between the electron temperatures, and a ~20% difference in the ion temperatures. Such large temperature

differences should be measurable with Thomson scattering [11], which would differentiate the electron-ion temperature equilibration models discussed in this paper.

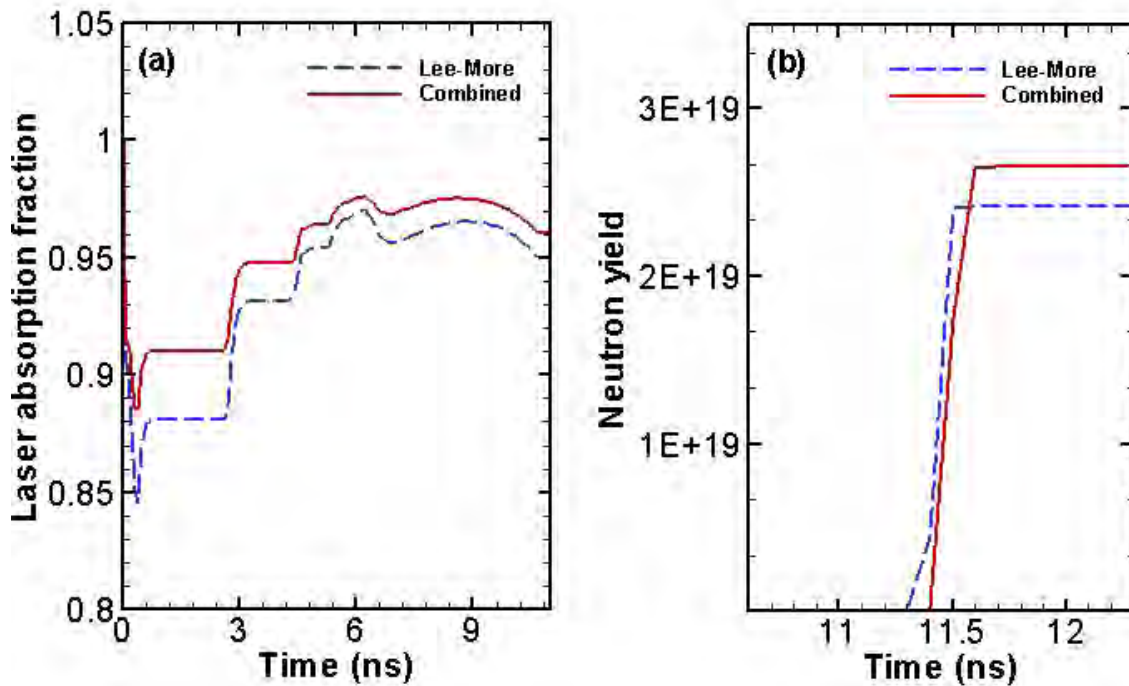


Figure 8 The proposed model compared with the Lee-More model for NIF designs

These graphs show a) the laser absorption and b) the neutron yield for the NIF designs. Based on how close the laser absorptions are, it is understandable that the neutron yields are relatively close together.

Similar simulations have also been performed for the NIF design, using the pulse shape in Fig. 4(a). The combined model predicts ~2% higher laser absorption; this small increase is expected because of the high absorption achieved on the NIF. This leads to the Combined model predicting only ~10% more neutron yield than the Lee-More model, seen in Fig. 8. A higher neutron yield is predicted because the Combined model takes into account the many-bodied effects of the shell better than the Lee-More model.

For the NIF designs, the Combined model predicts higher electron and ion temperatures, Fig. 9, than the Lee-More model. The final target gain predicted by the Combined model is 49.8, which is ~10% higher than the 45.5 gain predicted by the Lee-More model.

Based on the results, the Combined model appears to be more effective at predicting the conditions during ICF fusion. This is based on the fact that it incorporates both classical and quantum mechanics effects.

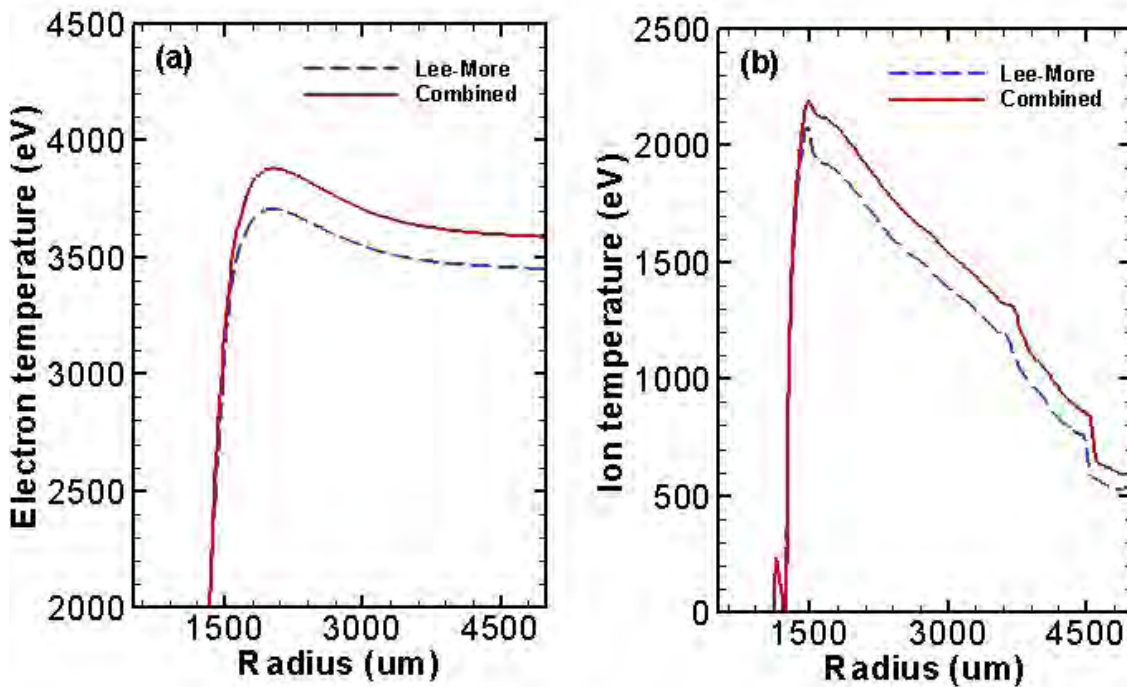


Figure 9 The electron and ion temperature compared for both models for the NIF
 These graphs show a) the electron temperatures and b) the ion temperatures as functions of radius.

4 Conclusion

Electron-ion temperature equilibration effects on cryogenic DT implosions on the OMEGA system and the NIF designs have been investigated. Different electron-ion relaxation models have been examined. A subroutine for the hydro-code, LILAC, was written to implement each of the four models.

The hydro-simulations have shown that there are distinct variations between the four models that are readily noticeable in experiments. The implosion performance is sensitive to the electron-ion temperature equilibration models because the inverse bremsstrahlung laser absorption is closely related to the electron-ion Coulomb logarithm and the coronal temperatures.

These calculations have shown that the Spitzer and Lee-More models predict too high and too low Coulomb logarithms, respectively. The MD model is best for modeling regions with densities less than the critical density, due to the use of the classical Newtonian model, while the BPS model is better suited for higher densities due to the incorporation of quantum mechanics effects.

As a result of these calculations, a piece-wise model was proposed to model the Coulomb logarithm most effectively. The piece-wise model comprised the classical MD model for the coronal plasma and the “hotspot”, and the BPS model for the shell conditions using quantum effects. This ensures that the most accurate results are calculated.

Moving forward, the accuracy of this model can be confirmed using Thomson scattering, which would differentiate between the models based on the electron and ion temperatures calculated. Finally, to ensure that this model remains as accurate as possible, it should be revisited and re-analyzed with every new model of the Coulomb logarithm that is constructed and proposed.

Acknowledgements:

I would like to thank Dr. S.X. Hu for being my research advisor for this project, Dr. R.S. Craxton for reviewing my figures and suggesting improvements, and the University of Rochester Laboratory for Laser Energetics for allowing me to use their facilities.

Bibliography

- [1] S. Atzeni and J. Meyer-ter-Vehn, *The Physics of Inertial Fusion*. Oxford. Clarendon Press. 2004.
- [2] J.D. Lindl, *Inertial Confinement Fusion: The Quest for Ignition and Energy Gain Using Indirect Drive*. New York. Springer-Verlag. 1998.
- [3] L. Spitzer, *Physics of Fully Ionized Gases*. New York. John Wiley & Sons, Inc. 1962.
- [4] G. Dimonte and J. Daligault, “Molecular-Dynamics Simulations of Electron-Ion Temperature Relaxation in a Classical Coulomb Plasma” *Physics Review Letters*, vol. 101, 135001. September, 2008.
- [5] Y.T. Lee and R.M. More. “An electron conductivity model for dense plasmas” *Physics of Fluids*, vol 27, 1273. December, 1983
- [6] L.S. Brown and R.L. Singleton, Jr. “Temperature equilibration in a fully ionized plasma: Electron-ion mass ratio effects” *Physics Review E*, vol. 79, 066407. June 2009.
- [7] J. Delettrez *et al.*, “Effect of laser illumination nonuniformity on the analysis of time-resolved x-ray measurements in uv spherical transport experiments” *Physics Review A*, vol. 36, 3926. October, 1987.
- [8] P.B. Radha *et al.* “Multidimensional analysis of direct-drive, plastic-shell implosions on OMEGA”. *Physics of Plasmas*, vol. 12, 056307. April, 2005.
- [9] S.X. Hu, B. Militzer, V.N. Goncharov, and S. Skupsky “Strong Coupling Effects and Degeneracy Effects in Inertial Confinement Fusion Implosions”. *Physics Review Letters*, vol. 104, 235003. June, 2010.
- [10] V.N. Goncharov, et al. “Demonstration of the Highest Deuterium-Tritium Areal Density Using Multiple-Picket Cryogenic Designs on OMEGA” *Physics Review Letters*, vol. 104, 165001. April, 2010.
- [11] D.H. Froula et al., “Quenching of the Nonlocal Electron Heat Transport by Large External Magnetic Fields in a Laser-Produced Plasma Measured with Imaging Thomson Scattering” *Physics Review Letters*, vol. 98, 135001. March, 2007.